AAS 14-331

COLLISION AVOIDANCE MANEUVER DESIGN BASED ON MULTI-OBJECTIVE OPTIMIZATION

Alessandro Morselli[*], Roberto Armellin[†], Pierluigi Di Lizia[‡], Franco Bernelli-Zazzera[§]

The possibility of having collision between a satellite and a space debris or another satellite is becoming frequent. The amount of propellant is directly related to a satellite's operational lifetime and revenue. Thus, collision avoidance maneuvers should be performed in the most efficient and effective manner possible. In this work the problem is formulated as a multi-objective optimization. The first objective is the the Δv, whereas the second and third one are the collision probability and relative distance between the satellite and the threatening object in a given time window after the maneuver. This is to take into account that multiple conjunctions might occur in the short-term. This is particularly true for the GEO regime, where close conjunction between a pair of object can occur approximately every 12h for a few days. Thus, a CAM can in principle reduce the collision probability for one event, but significantly increase it for others. Another objective function is then added to manage mission constraint. To evaluate the objective function, the TLE are propagated with SGP4/SDP4 to the current time of the maneuver, then the Δv is applied. This allow to compute the corresponding "modified" TLE after the maneuver and identify (in a given time window after the CAM) all the relative minima of the squared distance between the spacecraft and the approaching object, by solving a global optimization problem rigorously by means of the verified global optimizer COSY-GO. Finally the collision probability for the sieved encounters can be computed. A Multi-Objective Particle Swarm Optimizer is used to compute the set of Pareto optimal solutions.

The method has been applied to two test cases, one that considers a conjunction in GEO and another in LEO. Results show that, in particular for the GEO case, considering all the possible conjunctions after one week of the execution of a CAM can prevent the occurrence of new close encounters in the short-term.

INTRODUCTION

The increasing number of resident space objects is impacting on the number of close conjunction that are occurring between objects in orbit around the Earth. Many efforts in the past years have thus been directed towards the research of new methods for the identification of close approaches, risk analysis, and design of escape maneuvers. In the case of a predicted high risk event, the possibility of a Collision Avoidance Maneuver (CAM) is considered. The classification of high-risk conjunctions depends on conjunction geometry, collision probability value, and satellite operator practice and procedures. These factors should be defined with the aim of avoiding all unnecessary CAM, to save

[*]PhD student, Department of Aerospace Science and Technology, Politecnico di Milano, 20156 Milan, Italy
[†]Lecturer in Astronautics, School of Engineering Sciences, University of Southampton, Southampton, SO17 1BJ, UK
[‡]Postdoctoral Fellow, Department of Aerospace Science and Technology, Politecnico di Milano, 20156 Milan, Italy
[§]Full professor, Department of Aerospace Science and Technology, Politecnico di Milano, 20156 Milan, Italy

fuel and in turns to guarantee satellite expected lifetime. When the driving parameters suggests that an event will exceed an admissible level of risk, a CAM is designed.[1,2] The aim of the maneuver is to increase the separation between the objects, in order to reduce the collision risk. The fuel consumption should be as low as possible and the spacecraft must be kept in the operational window.

When the threatening conjunction occurs close to a designed station keeping maneuver, it can be sufficient to anticipate it to reach an acceptable level of risk. The advantage of this approach is that no extra fuel has to be used for an ad-hoc maneuver and mission constraints are not violated. In all other cases a CAM (and maybe a subsequent restitution maneuver) has to be designed. Using along-track burns it is possible to raise or decrease the altitude of the object at the time of the conjunction or, with lower Δv, to bring forward or delay the arrival at the conjunction location.[3] The first strategy has to be applied with head-on conjunction, whereas the second is suitable for an oblique approach geometry.

CAM can be optimized by looking at the gradient of the collision probability with respect to velocity increment component and then using numerical methods to find the Δv that lowers the collision probability up to the desired value.[4] Analytical expressions of the relative Keplerian dynamics of the two bodies on the B-plane can be obtained and used to set-up an optimization of the Δv to maximize the collision miss distance.[5]

The design of CAM can be also tackled as an optimization problem. Genetic Algorithms (GA) were used for the design of CAM for LEO and GEO objects, taking into account mission constraints and combining them into a single objective function to be minimized.[6] More complex cases, such as the presence of multiple objects, can be tackled by GA optimization of the maneuver. In that case the use of an along-track maneuver can not be the optimal choice to reduce collision risk.[7]

In this paper we assess the CAM design as a multi-objective optimization problem, using a Multi-Objective Particle Swarm Optimizer (MOPSO).[8] In this way, it is possible to define a set of objective functions, each one targeted for a particular constraint (e.g. ground track repeatability), or optimization objective (e.g. minimum fuel consumption and collision risk reduction) without the need of combining all of them in a single one using scaling factors. Furthermore, the optimization will provide a set of solutions that are Pareto efficient, i.e. each CAM belonging to this set is such that any change in it will result in a worst performance in one or more objective functions. The set of all Pareto efficient solution is usually referred to as "Pareto front". The analyst can then select a CAM on the Pareto front, e.g. the one that guarantees a reduction of collision risk up to an acceptable level. This is not possible for a single-objective optimization that provides only one optimal solution that is strongly dependent on the scaling factors that are, in case, used to assemble objective functions.

The paper is organized as follows: first we describe the method we use for the identification of conjunction and to compute the probability of collision between the two objects. We also provide details on Differential Algebra and the rigorous global optimizer COSY-GO, that are the key elements for our conjunction identification and algorithm. Then, we describe how the Collision Avoidance Maneuver (CAM) is optimized, focusing on the selected optimization algorithm and the design of the objective functions. Subsequently, we analyze two test cases, one considering two LEO objects and the other two GEO objects, and try to identify the performances of the method. A critical discussion of the results is then made before conclusions and future developments.

IDENTIFICATION OF CONJUNCTION AND COLLISION PROBABILITY

In this section we describe how we compute a potential conjunction and the associated collision probability. These two procedures are the cornerstones of the CAM optimization, that will be described later. The conjunction identification is tackled as a global optimization problem, using an optimizer based on Taylor models that can provides sharp, rigorous enclosures of the minima.[9] A brief description of Taylor models and differential algebra is provided together with a few details on the global optimizer COSY-GO. Subsequently, a few notes on collision probability computation are given and the selected method is specified.

Notes on Taylor models

Verified global optimization needs the determination of rigorous upper and lower bounds of the objective function in order to implement a branch-and-bound method.[10] The commonly used interval approach has excelled in solving this problem elegantly from both a formal and an implementational viewpoint. However, there are situations where the method has limitations for extended or complicated calculations because of the dependency problem, which is characterized by a cancellation of various sub-parts of the function that cannot be detected by direct use of interval methods. This effect often leads to pessimism and sometimes even drastic overestimation of range enclosure. Furthermore, the sharpness of intervals resulting from calculations typically scales linearly with the sharpness of the initial discretization intervals. For complicated problems, and in particular higher dimensions, this sometimes significantly limits the sharpness of the resulting answer that can be obtained.[11]

The Taylor model approach enables the computation of fully mathematically rigorous range enclosures while largely avoiding many of the limitations of the conventional interval method.[12] The method is based on the inductive local modeling of functional dependencies by a polynomial with a rigorous remainder bound, and as such represents a hybrid between formula manipulation, interval methods, and methods of computational differentiation.[13,14]

An n-th order Taylor model of a multivariate function f that is $(n+1)$ times continuously partially differentiable on the domain D, consists of the n-th order multivariate Taylor polynomial P expanded around a point $\boldsymbol{x}_0 \in D$ and representing a high-order approximation of the function f, and a remainder error interval I for verification such that

$$\forall \boldsymbol{x} \in D, \quad f(\boldsymbol{x}) \in P(\boldsymbol{x} - \boldsymbol{x}_0) + I. \tag{1}$$

From Taylor's theorem, it is clear that the width of the remainder interval I can be chosen to scale with the domain size proportional to $|\boldsymbol{x} - \boldsymbol{x}_0|^{n+1}$. The practical computation of P and I is based on Taylor model arithmetic, which carries P and I trough all the operations comprising I. By choosing the size $|\boldsymbol{x} - \boldsymbol{x}_0|$ sufficiently small and the order n sufficiently high, the size of the remainder interval I can be kept very small in practice. The bulk of the functional dependency is kept in the polynomial part P with point coefficients, and there is no interval arithmetic associated inflation that happens in the polynomial part. Thus, the interval related overestimation is rather optimally suppressed with the Taylor model method.[11] The implementation of the method in the code COSY INFINITY[12,15] supports binary operations and standard intrinsic functions, as well as the antiderivative operation which widens the applications of the method. Note that when only the polynomial part P of the Taylor model is considered, also the analytic operation of differentiation can be introduced, so finalizing the definition of a differential algebraic (DA) structure.[16]

The Taylor model approach has the following important properties:

1. The ability to provide rigorous enclosures of any function given by a finite computer code list by a Taylor polynomial and a remainder bound with a sharpness that scales with order $(n+1)$ of the width of the domain.

2. The computational expense increases only moderately with order, allowing the computation of sharp range enclosures even for complicated functional dependencies with significant dependency problem.

3. The computational expense of higher dimensions increases only very moderately, significantly reducing the "curse of dimensionality".

The structure of Taylor models naturally represents a rich resource of information. In particular, the coefficients of the polynomial part P of a Taylor model are nothing but the derivatives up to order n. Consequently, when representing a function f by a Taylor model $P + I$ on a computer, we also obtain the local slope, Hessian and higher order derivatives. When a task is focused on range bounding, those pieces of information become particularly useful.

While naive range bounding of Taylor models, namely merely evaluating each monomial of P using interval arithmetic then summing up all the contributions as well as the remainder interval I,[17] already exhibits the superiority over the mere interval arithmetic and the more advanced centered form,[12] the active utilization of those additional pieces of information in Taylor models has a lot of potential of developing efficient range bounders. Based on this observation, various kinds of Taylor model based range bounders have been developed,[18] and among them the linear dominated bounder (LDB) and the quadratic fast bounder (QFB) are the backbones of Taylor model based verified global optimizer COSY-GO that will be discussed afterward.

The linear dominated bounder is based on the fact that for Taylor models with sufficiently small remainder bound, the linear part of the Taylor model dominates the behavior, and this is also the case for range bounding. The linear dominated bounder utilizes the linear part as a guideline for iterative domain reduction to bound Taylor models. Around an isolated interior minimizer, the Hessian of a function f is positive definite, so the purely quadratic part of a Taylor model (P, I) which locally represents f, has a positive definite Hessian matrix H. The quadratic fast bounder provides a lower bound of a Taylor model cheaply when the purely quadratic part is positive definite. More details on polynomial bounders are given in Reference 19.

COSY-GO

COSY-GO[18] is a branch-and-bound optimization algorithm employing local domain reduction techniques exploiting the bounding performances assured by Taylor model methods. Should the global minimum of a sufficiently regular scalar function f on a given domain $A \subseteq \mathbb{R}^m$ wished to be evaluated, the algorithm starts with an initial value for the global optimum, the *cutoff* value, and then proceeds on analyzing at each step a sub-domain for possible elimination or reduction. At each step the following tasks are performed

1. A rigorous lower bound l of the objective function is obtained on the sub-domain of interest using various bounding schemes hierarchically with the hope of showing that l lies above the already established cutoff value, which will allow elimination of the sub-domain. A first

assessment is made whether the remainder bound of the Taylor model at hand is sufficiently small; if it is not, then the underlying function exhibits too much detail for modeling by local estimators, and the sub-domain is split in the direction of fastest change of the function.

2. If the remainder bound is sufficiently small, as a first test the polynomial part of the objective function is evaluated in interval arithmetic. When it fails to eliminate the box, the LDB bounder is applied. If it also fails to eliminate the box, and if the quadratic part of the polynomial representation of the objective function P is positive definite, the QFB bounder is applied.

3. If the just studied sub-domain of interest cannot be eliminated, but is seen to have a lower bound close to the current cutoff values, domain reduction techniques are brought to bear based on the LDB and QFB algorithms to reduce the sub-domain in size. Once these methods are applicable, they will allow to cut the sub-domain of interest and rapidly reduce the active volume.

4. The cutoff value is updated using various schemes. First, the linear and quadratic parts of the Taylor polynomial are utilized to obtain a potential cutoff update. In particular, if the quadratic part of the polynomial is positive definite, the minimizer of the quadratic polynomial is tested. If the quadratic part is not positive definite, the minimizer of the quadratic part in the direction of the negative gradient is tested. For objective functions of nontrivial cost, as in the example at hand, also more sophisticated local searches within and near the current sub-domain may be carried out.

The algorithm continues to reduce and examine the domain until the minimum dimension allowed is reached. The result of the optimization is the validated enclosure of the global minimum of the problem.

Conjunction Determination

The computation of the time of closest approach (TCA) and distance of closest approach (DCA) between two space bodies in a given time window can be formulated as an optimization problem in which the global minimum of the square distance function between the two orbiting bodies is searched.[9] In general, given the initial set of orbital elements $\boldsymbol{e}^0$ at epoch t^0, the state of a body at time t can be expressed as

$$\boldsymbol{x} = \boldsymbol{g}(\boldsymbol{e}^0, t), \tag{2}$$

where $\boldsymbol{x} = (\boldsymbol{r}, \boldsymbol{v})$ and $\boldsymbol{g}$ is a nonlinear function that maps the initial orbital elements in the final state. Thus, $\boldsymbol{g}$ includes both coordinate transformations and the forward propagation of the state up to time t. For SGP4/SDP4 algorithm, $\boldsymbol{e}^0$ is the vector of mean elements included in the TLE. The procedure to compute the state $\boldsymbol{x}$ can be summarized in

1. Recover Brouwer mean motion from the Kozai mean motion included in the TLE.

2. Update orbital elements at time t adding secular effects of Earth's zonal harmonics and lunisolar perturbations.

3. Compute resonance effect of Earth's gravity through numerical integration.

4. Add long-period periodic perturbation due to Moon's, Sun's, and Earth's gravity.

5. Solve Kepler's equation for $U = E + \omega$.

6. Update for short-periodic effects of Earth's gravity.

7. Compute $\boldsymbol{x}$ from the updated Keplerian elements.

For details on the Taylor model evaluation of SGP4/SDP4 please refer to 9.

The computation of the DCA and TCA is addressed as a global optimization problem in which the square of the distance function is the objective function to be minimized

$$J_{GM}(t) = d(t)^2 = (\boldsymbol{r}_2 - \boldsymbol{r}_1) \cdot (\boldsymbol{r}_2 - \boldsymbol{r}_1). \tag{3}$$

For problems of practical interest the computation of all the minima of the square distance function can be important, as a local minimum occurring before the TCA can potentially represent a risky condition (this is particularly true when models accuracy and uncertainties on orbit determination are taken into account). When all the minima are searched for, firstly the time derivative of the square distance is computed

$$\frac{\mathrm{d}d(t)^2}{\mathrm{d}t} = 2d\dot{d} = 2(\boldsymbol{v}_2 - \boldsymbol{v}_1) \cdot (\boldsymbol{r}_2 - \boldsymbol{r}_1), \tag{4}$$

then the objective function is set to

$$J_{SP}(t) = [(\boldsymbol{v}_2 - \boldsymbol{v}_1) \cdot (\boldsymbol{r}_2 - \boldsymbol{r}_1)]^2. \tag{5}$$

Note that Eq. (5) is positive semidefinite, and its zeros (i.e. its global minima) are stationary points of the distance function. These stationary points are then classified by exploiting the high order derivatives included in the polynomial part of the Taylor model. The procedure for the CAM optimization will use this approach to compute all local minima within the desired time window.

COMPUTATION OF COLLISION PROBABILITY

The collision probability is an important measure of the level of risk of a close encounter. The uncertainties in position and velocities coming from orbit determination can be translated into a probability density function that describes the orbital state of each object at the nominal TCA The probability density function is then integrated over the volume V_c given by the shapes of the satellite and colliding object to retrieve the collision probability.

Different methods exist for the computation of this multi-dimensional integral. Most of these approaches have the following assumptions in common:[20,21,22]

- Position uncertainties of the two objects are not correlated;
- Objects move along straight lines at constant velocity during the conjunction;
- The uncertainties in the velocities can be neglected;
- Position uncertainty during the encounter is constant and equal to the value at estimated conjunction;
- The uncertainties in the positions of the two objects are represented by three-dimensional Gaussian distributions.

These assumptions are suitable for most close approaches, since the duration of the encounter usually lasts a few seconds and conjunction occur only a few days after the reference epoch so that the uncertainty on position can be still considered Gaussian. The initial uncertainty can be expressed by means of a (6×6) covariance matrix C_0 that can be propagated to the TCA using a state covariance matrix, $\mathbf{\Phi}(t)$:

$$\boldsymbol{C}(t) = \mathbf{\Phi}(t)\, \boldsymbol{C}_0\, \mathbf{\Phi}^T(t). \tag{6}$$

The covariance matrix can be easily computed by means of the automatic differentiation techniques made available by COSY INFINITY. Once an arbitrary set of orbital elements is chosen, a DA initialization of these uncertain variables can be performed. As an example, uncertainty of TLE can be estimated in the RTN reference frame.[3,23] According to Figure 1, the first unit vector of the reference frame $\hat{\boldsymbol{r}}$ is aligned with the position vector $\boldsymbol{r}$, the third unit vector $\hat{\boldsymbol{n}}$ is perpendicular to the orbital plane, and the second unit vector , or transverse unit vector, $\hat{\boldsymbol{t}}$ completes the frame. Note that this unit vector is aligned with satellite velocity only for circular orbits.

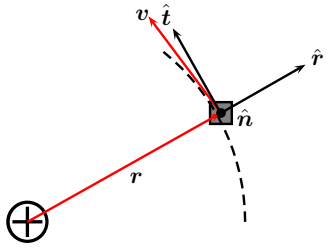

Figure 1. RTN reference frame, radial $\hat{r}$, transverse $\hat{t}$, and normal $\hat{n}$ vectors.

Since TLE and SGP4/SDP4, used for orbit propagation in this work, are written in classical orbital elements, the relations between RTN state vector and Keplerian orbital elements is found through the following steps:

1. Compute TEME state vector $\boldsymbol{x} = [\boldsymbol{r}; \boldsymbol{v}]$ at TLE epoch. This is achieved with an evaluation of SGP4/SDP4 at time 0.0
$$[\delta \boldsymbol{x}_0] = [\mathcal{M}_{\text{TEME}}]\, [\delta \boldsymbol{\kappa}_0]\,, \tag{7}$$
where $\boldsymbol{\kappa}_0$ is the classical orbital element vector $\boldsymbol{\kappa} = \{a, e, I, \Omega, \omega, M\}^T$

2. Convert TEME vectors into ECI J2000 vectors, retrieving
$$[\delta \boldsymbol{x}_{0,\text{ECI}}] = [\mathcal{M}_{\text{ECI}}]\, [\delta \boldsymbol{\kappa}_0] \tag{8}$$

3. Transform ECI J2000 state vector into RTN orbital frame, obtaining
$$[\delta \boldsymbol{x}_{0,\text{RTN}}] = [\mathcal{M}_{\text{RTN}}]\, [\delta \boldsymbol{\kappa}_0] \tag{9}$$
This map provides the RTN initial state deviation as function of classical orbital elements variation.

4. Invert the DA map with DA tools, retrieving
$$[\delta \boldsymbol{\kappa}_0] = [\mathcal{M}_{\text{RTN}}]^{-1}\, [\delta \boldsymbol{x}_{0,\text{RTN}}] \tag{10}$$

The obtained DA map describes the deviation of the mean orbital elements used in SGP4/SDP4, as function of deviation from position and velocity in RTN frame. By plugging this transformation in the SGP4/SDP4 initialization phase, it is possible to compute the object position $\boldsymbol{r}_f$ and velocity $\boldsymbol{v}_f$ in TEME reference frame as a function of initial uncertainties by simply evaluating the COSY INFINITY implementation of SGP4/SDP4 at the desired time. It is then straightforward to assembly the state transition matrix by computing the first derivatives with respect to the initial uncertain variables within the DA framework

$$\boldsymbol{\Phi}(t) = \begin{bmatrix} \dfrac{\partial \boldsymbol{r}_f}{\partial \boldsymbol{r}^T_{0,\text{RTN}}} & \dfrac{\partial \boldsymbol{r}_f}{\partial \boldsymbol{v}^T_{0,\text{RTN}}} \\ \dfrac{\partial \boldsymbol{v}_f}{\partial \boldsymbol{r}^T_{0,\text{RTN}}} & \dfrac{\partial \boldsymbol{v}_f}{\partial \boldsymbol{v}^T_{0,\text{RTN}}} \end{bmatrix}. \tag{11}$$

The covariance matrices, $\boldsymbol{C}^1_{6\times6}$ and $\boldsymbol{C}^2_{6\times6}$, of the two object involved in the close approach are thus propagated to the TCA using Eq. (6) and the state transition matrices computed using the above procedure. The combined covariance matrix $\boldsymbol{C}$ is given by

$$\boldsymbol{C}_{6\times6} = \boldsymbol{C}^1_{6\times6} + \boldsymbol{C}^2_{6\times6} \tag{12}$$

because, by hypothesis, the uncertainties of the two objects are not correlated. The 3×3 submatrix corresponding to the uncertainty in the final position is then extracted, since uncertainty on velocity are assumed to be negligible. The combined probability density function of the relative position vector is thus expressed as a Gaussian distribution by

$$p\left(\Delta\boldsymbol{r}\right) = \frac{1}{\sqrt{(2\pi)^3 \det \boldsymbol{C}_{3\times3}}} e^{-\frac{1}{2}\Delta\boldsymbol{r}^T \boldsymbol{C}^{-1}_{3\times3}\Delta\boldsymbol{r}}, \tag{13}$$

where $\Delta\boldsymbol{r}$ is the objects relative position vector. The collision probability of the encounter P_c is given by the integral over the combined hard body volume of the two objects, V_c, of the probability density function

$$P_c = \frac{1}{\sqrt{(2\pi)^3 \det \boldsymbol{C}_{3\times3}}} \iiint_{V_c} e^{-\frac{1}{2}\Delta\boldsymbol{r}^T \boldsymbol{C}^{-1}_{3\times3}\Delta\boldsymbol{r}}\, dV. \tag{14}$$

The volume integral can be reduced to a surface integral on the B-plane, that is perpendicular to the relative velocity $\Delta\boldsymbol{v}$ at the TCA. The two unit vectors

$$\boldsymbol{X}_b = \frac{\Delta\boldsymbol{r}}{|\Delta\boldsymbol{r}|}; \quad \boldsymbol{Y}_b = \frac{\Delta\boldsymbol{r} \times \Delta\boldsymbol{v}}{|\Delta\boldsymbol{r} \times \Delta\boldsymbol{v}|}, \tag{15}$$

define the two perpendicular axis belonging to the B-plane and are used to build a transformation matrix, $\boldsymbol{R}_b$, from TEME to B-plane reference frame

$$\boldsymbol{R}_b = \begin{bmatrix} \boldsymbol{X}^T_b \\ \boldsymbol{Y}^T_b \end{bmatrix}. \tag{16}$$

The 2×2 projected covariance matrix is computed by means of

$$\boldsymbol{C}_b = \boldsymbol{R}_b\, \boldsymbol{C}_{3\times3}\, \boldsymbol{R}^T_b \tag{17}$$

The volume integral is then reduced to a 2D integral over the combined cross-section circle of radius D, centered at the predicted $\Delta \boldsymbol{r}_b = \boldsymbol{R}_b \Delta \boldsymbol{r}$

$$P_c = \frac{1}{2\pi\sqrt{\det \boldsymbol{C}_b}} \int_{-D}^{D} \int_{-\sqrt{D^2-x_b^2}}^{\sqrt{D^2-x_b}} e^{-\frac{1}{2}\Delta \boldsymbol{r}_b^T \boldsymbol{C}_b^{-1} \Delta \boldsymbol{r}_b} \, dy_b \, dx_b. \tag{18}$$

If the reference frame is oriented as the major and minor axis of the covariance ellipse on the B-plane, the integral becomes

$$P_c = \frac{1}{2\pi \, \sigma_x \, \sigma_y} \int_{-D}^{D} \int_{-\sqrt{D^2-x^2}}^{\sqrt{D^2-x^2}} e^{-\frac{1}{2}\left[\left(\frac{x+x_m}{\sigma_x}\right)^2 + \left(\frac{y+y_m}{\sigma_y}\right)^2\right]} \, dy \, dx, \tag{19}$$

where σ_x and σ_y are the standard deviations of the minor and major axis respectively, and the position of the chaser in the covariance frame is given by x_m and y_m. Alfano[24] expressed the former integral as a combination of error functions and exponential terms of the form

$$\begin{aligned} P_c = \frac{2D}{\sigma_x n \sqrt{8\pi}} \sum_{i=0}^{n} \Bigg[& \operatorname{erf}\left(\frac{y_m + \frac{2D}{n}\sqrt{(n-i)\, i}}{\sigma_y \sqrt{2}} \right) + \\ & + \operatorname{erf}\left(\frac{-y_m + \frac{2D}{n}\sqrt{(n-i)\, i}}{\sigma_y \sqrt{2}} \right) \exp\left(- \frac{\left(\frac{2i-n}{n} D + x_m\right)^2}{2\sigma_x^2} \right) \Bigg]. \end{aligned} \tag{20}$$

The series of Eq. (20) is used to compute collision probability for close encounters throughout this work, using a number of terms $n = 100$.

CAM OPTIMIZATION

The following criteria are considered as driving factors for the CAM optimization

- Minimize fuel consumption
- Increase separation between the two objects
- Decrease collision risk below an accepted value
- Avoid that CAM increases the collision probability of other conjunctions in the week following the maneuver
- No violation of mission constraints for the target within a given time window

In order to use classic optimization codes (i.e. gradient based methods) to solve a multi-objective optimization problem, a common practice is to merge the different objective functions into a single scalar objective function by means of weighting factors. This technique requires an accurate selection of the weights, and it has, as major drawback, the identification of a single optimal solution per

run. It is clear that it is difficult to define a single objective function that takes into account all the criteria previously listed. For this reason the CAM design is here tackled as a multi-objective optimization problem. The advantage of a multi-objective optimization is that it can manage a vector of objective functions, retrieving a set of Pareto optimal solutions. In the following, a few details on the population-based optimizer MOPSO are given and the optimization strategy and architecture are described.

MOPSO

Population-based optimizers can be easily modified to deal with a vector of objective functions delivering the entire set of Pareto optimal solutions. Furthermore, particle swarm optimization seems particularly suitable for multi-objective optimization mainly because of the high speed of convergence that the algorithm presents for single-objective optimization.[8] In a multi-objective optimization problem the objective function is a M dimensional vector

$$\boldsymbol{f}(\boldsymbol{x}) = (f_1(\boldsymbol{x}), f_2(\boldsymbol{x}), \ldots, f_M(\boldsymbol{x}))\,. \tag{21}$$

In this frame, a criterion to compare vectors is necessary to identify the optimal solution set. The Pareto dominance is the appropriate criterion to serve this aim, enabling the solutions ranking.[25]

The MOPSO implemented for the solution of the problem at hand is based on the following algorithmic flow:

1. Randomly initialize a number of individuals or particles N within the design space.

2. Evaluate the objective function

$$\boldsymbol{y}_i = \boldsymbol{f}(\boldsymbol{x}_i) \quad \text{for} \quad i = 1, \ldots, N. \tag{22}$$

3. Update the personal best solution $\boldsymbol{p}_{\text{best}}$. The solutions are compared using the Pareto dominance criterion. Thus for each particle we have

$$\boldsymbol{p}_{\text{best}} = \begin{cases} \boldsymbol{x}_i & \text{if } \boldsymbol{x}_i \text{ dominates } \boldsymbol{p}_{\text{best}} \\ \boldsymbol{p}_{\text{best}} & \text{if } \boldsymbol{p}_{\text{best}} \text{ dominates } \boldsymbol{x}_i \\ \boldsymbol{x}_i \text{ or } \boldsymbol{p}_{\text{best}} \text{ randomly} & \text{in the other cases} \end{cases} \quad \text{for } i = 1, \ldots, N\,. \tag{23}$$

4. Update global best list $\boldsymbol{G}_{\text{best}}$. In the multi-objective problem $\boldsymbol{G}_{\text{best}}$ is the analogous of the scalar global best $\boldsymbol{g}_{\text{best}}$ and it represents the entire set of non-dominated solutions. This list is updated by processing the subset of non-dominated solutions $\boldsymbol{x}_j$ with $j = 1, \ldots, N^* \leq N$

   - If $\boldsymbol{x}_j$ is dominated by one of the solution belonging to the list, do not updated the list
   - If $\boldsymbol{x}_j$ dominates one or more solutions belonging to the list, then add $\boldsymbol{x}_j$ to the $\boldsymbol{G}_{\text{best}}$ list and delete the dominated solutions
   - If $\boldsymbol{x}_j$ neither dominates nor is dominated by any solution belonging to the $\boldsymbol{G}_{\text{best}}$ list, then simply add $\boldsymbol{x}_j$ to the list

5. Update the global best solution $\boldsymbol{g}_{\text{best}}$. Note that the $\boldsymbol{g}_{\text{best}}$ is univocally defined for a scalar objective function, whereas it must be opportunely chosen within the $\boldsymbol{G}_{\text{best}}$ list in the multi-objective case. The selection of the $\boldsymbol{g}_{\text{best}}$ plays a key role in obtaining a uniform set of Pareto

optimal solutions. For this purpose a uniform 30 cells grid in the objective space is defined at each iteration and the number of solutions belonging to each grid cell is calculated. Based on this number, a roulette-wheel method is then applied to promote the selection of $\boldsymbol{g}_{\text{best}}$ in a low populated grid-cell.

6. Compute the new particles position by

$$\boldsymbol{x}_i^{k+1} = \boldsymbol{x}_i^k + \boldsymbol{v}_i^{k+1}\Delta t \quad \text{for} \quad i = 1, \ldots, N, \tag{24}$$

in which $\boldsymbol{v}_i^{k+1}$ is the velocity of the i-th particle at the $(k+1)$ iteration, given by

$$\boldsymbol{v}_i^{k+1} = w\boldsymbol{v}_i^k + c_1 r_1 \frac{\boldsymbol{x_i^k} - \boldsymbol{p}_{\text{best}}}{\Delta t} + c_2 r_2 \frac{\boldsymbol{x_i^k} - \boldsymbol{g}_{\text{best}}}{\Delta t}. \tag{25}$$

7. Repeat 2-6 until the convergence criterion is satisfied or the maximum number of iterations is reached.

The parameters c_1 and c_2 of Eq. (25) are considered constant and equal to 2 during the optimization, assuring a balance between local and global terms. A linear decrease of w with the iteration number in the interval $[0.4, 1.4]$ is adopted. In particular a greater value of the inertia enables a better exploration of the search domain in the first phase of the optimization, whereas a lower value allows a better analysis of the most promising areas of research space in the subsequent phases. Note that if the position of a particle goes outside the search space, the violated component of the decision vector takes the value of the corresponding boundary and its velocity component is multiplied by a random number between $[-1, 0]$.

The maximum numbers of particle belonging to the $\boldsymbol{G}_{\text{best}}$ is fixed to 100 units. The same procedure adopted for selecting the $\boldsymbol{g}_{\text{best}}$ is used to delete those solutions belonging to a highly populated grid-cell, if the maximum list size is exceeded.

The problem addressed with implemented MOPSO is characterized by the presence of inequality constraints necessary to control the time of execution of the CAM and limit the $\Delta\boldsymbol{v}$ in terms of module and direction. As the feasible domain inside the search space is sufficiently large the feasible solution method (FSM) is adopted for the constraints handling.[26] More specifically the swarm initialization is performed randomly, but only feasible solutions are retained. This implies that the first step of the algorithm generally requires the evaluation of a number of solutions greater than the population size. Furthermore, only feasible solutions are counted for the $\boldsymbol{g}_{\text{best}}$ and $\boldsymbol{p}_{\text{best}}$ values during the optimization. The initial velocity of the particle is set to be 0.

The convergence criterion adopted is based on the comparison of the average position of the non dominated solutions in the objective space with the same average position of the previous 20 iterations. If the component-wise difference of this two vectors is lower than 1% the Pareto set of optimal solutions is assumed to have been found. Furthermore, a maximum number of iterations of 20 and a 50 particle swarm are considered. These values are chosen, on the basis of several experiments, to assure an acceptable repeatability of the Pareto optimal solution set with a limited computational time.

Optimization strategy and architecture

Four free parameters are considered: the maneuver time t_m, the module of Δv, and its direction, expressed as a function of two angles λ and ϕ. The vector $\Delta\boldsymbol{v}$ is defined in the RTN reference frame

as

$$\Delta \boldsymbol{v} = \Delta v \begin{Bmatrix} \cos(\phi)\cos(\lambda) \\ \cos(\phi)\sin(\lambda) \\ \sin(\phi) \end{Bmatrix} \tag{26}$$

A set of these variables, hereafter grouped in the vector $\boldsymbol{x}$, univocally identifies a possible maneuver. Under the hypothesis of an instantaneous burn the orbital state after the maneuver is given by

$$\begin{Bmatrix} \boldsymbol{r}(t_m^+) \\ \boldsymbol{v}(t_m^+) \end{Bmatrix} = \begin{Bmatrix} \boldsymbol{r}(t_m^-) \\ \boldsymbol{v}(t_m^-) \end{Bmatrix} + \begin{Bmatrix} \mathbf{0} \\ \Delta \boldsymbol{v} \end{Bmatrix} \tag{27}$$

where the vector $\Delta \boldsymbol{v}$ is in TEME reference frame. By imposing the passage through the new state at t_m^+, the TLE of the target is updated. A new search for all minima in a time window of 7-days is the performed, starting from t_m. The search is performed as a global optimization problem with COSY-GO and using the SGP4/SDP4 analytical propagator. This allows for the computation of collision probability with Alfano's formula (Eq. (20)) for each minima whose associated relative distance is below the conjunction threshold. At this point, it is possible to define a set of objective functions, $\boldsymbol{f}(\boldsymbol{x})$, that are used by the optimizer to manage the plethora of design criteria. The objective function associated to propellant minimization is

$$f_1(\boldsymbol{x}) = \frac{\Delta v}{\Delta v_{\text{max}}} \tag{28}$$

where Δv_{max} corresponds to the maximum amount of fuel that can be allocated for the maneuver.

The second figure of merit is designed to increase both the closest approach distance and the distances of other conjunctions that may occur within the time window of interest $[t_m; t_m + 7]$. The objective function is defined as follows

$$f_2(\boldsymbol{x}) = \frac{1}{2}\,\frac{R - \min\left(d(t)\right)}{R} + \frac{1}{2}\,\frac{R - \overline{d}}{R}, \tag{29}$$

where $\min\left(d\right)$ is the distance of closest approach after the maneuver, and $\overline{d}$ is the mean distance of all local minima below the conjunction threshold R. When both the minimum and the mean value are equal to R the objective function has value zero. In case no minima below R are found the value of $f_2(\boldsymbol{x})$ can be set equal to zero. This combination is chosen to correctly handle situations in which using only mean or minimum is not sufficient. As an example, let us consider the case in which a very low global minima is found together with many other local minima close to the threshold R. By using only the mean value, $f_2(\boldsymbol{x})$ would result to be close to 1, since the global minima is diluted by the mean.

The third objective function involves the collision probability of the global minimum, and is

$$f_3(\boldsymbol{x}) = \log_{10}\left(P_c + 1\right). \tag{30}$$

This function is close to zero for little collision probabilities and reaches $\log_{10} 2$ when the collision probability is maximum. The lower the probability, the lower the objective function, the more the probability is close to 1 the more the value gets close to $\log_{10} 2$.

It could be observed that the two objective functions $f_2(\boldsymbol{x})$ and $f_3(\boldsymbol{x})$ could be condensed in a single one, by computing the P_c for all minima and compute the sum of all collision probabilities.

Anyway this would imply that a good knowledge of the orbital elements uncertainties is available during the considered time span for both the target and the chaser. This is usually not true when the chaser is a debris. In addition, the uncertainties grow with time if no other orbit determination is performed, resulting in possible underestimation of the actual collision probability. For this reason, we prefer to separate the objective functions.

To handle mission constraints, another objective function is introduced. The design of such a function is not straightforward, since each mission has different requirements and constraints. As an example, a GEO satellite should lie in a well-defined latitude and longitude slot, whereas a LEO satellite can have requirements on ground-track evolution. To avoid the definition of an ad-hoc objective function for each case we used the following definition

$$f_4(\boldsymbol{x}) = \frac{T_{\text{cycle}} - t_{in}}{T_{\text{cycle}}} \tag{31}$$

where T_{cycle} is the desired time for which the mission constraint are not violated and t_{in} is the actual time of violation. In this way, the user has to verify when the mission constraints are violated, e.g. performing an orbit propagation and comparing the latitude and longitude with their limit values.

To summarize, for each set of free parameters, the following steps are performed

1. Select the current particle $\boldsymbol{x}_i$
2. Update TLE of the target using the state after the implementation of the maneuver;
3. Perform a conjunction identification on a 7-days windows, starting from the maneuver epoch;
4. Find the global minimum and compute the mean of all minima below R;
5. Compute the collision probability using Alfano's method for the global minimum if below R;
6. Find the time for which mission constraints are violated, performing orbit propagation. The set of inequalities will change according to the mission constraints, which are different from mission to mission;
7. Compute the objective function vector $\boldsymbol{y} = \boldsymbol{f}(\boldsymbol{x_i})$.

In the following section the approach is applied to two test cases, one LEO and one GEO orbit.

TEST CASES

In this section the CAM optimization is applied to two orbital conjunction, one in the LEO and the other in the GEO regime. In both cases the conjunction threshold is $R = 10$ km and the hard-body radius for collision probability computation is $D = 100$ m. The collision threshold D is not related to body size in this case but guarantees that the collision probability for the nominal conjunction is above 10^{-4}. The upper and lower boundaries, u_b and l_b, of the optimization variables are listed in Table 1. No constraints on the maneuver direction are considered for these simulations and the time of the maneuver can occur up to one revolution before the targeted conjunction.

All computations are performed on an Intel Core i5 2500 @3.30GHz, 8Gb RAM processor running Sabayon Linux 13 (kernel version 3.11.0), each run of the MOPSO lasts approximately 2 h for both LEO and GEO cases.

Table 1. Upper and lower boundaries of optimization variables

Variable		l_b	u_b
t_m	(rev.)	0	1
Δv	(m/s)	0	1
λ	(deg)	0	360
ϕ	(deg)	-90	+90

LEO case

The LEO test case considers a close conjunction between satellite Metop-A and a debris from Iridium-33 (NORAD ID 33874) occuring at 23:58:12 UTC on 2012/03/02.[27] Metop-A is on a sun-synchronous orbit, with an altitude of 820 km and an inclination of 98.7 deg, and its repeat cycle is 29 days and 412 revolutions. Iridium-33 debris instead is found at an inclination of 86 deg, and has an apogee of 890 km and a perigee of 750 km. According to last TLE data* before the event, the DCA is 590 m, with a radial, along-track, and out-of-plane separation of 451, 222, and 308 m respectively. The relative velocity at the TCA, again computed using SGP4/SDP4 and COSY-GO, is 12 km/s, mainly distributed on the along-track (9.7 km/s) and out-of-plane (7.1 km/s) components. The nominal collision probability for the close conjunction is $P_c = 5.118 \times 10^{-4}$.

A CAM optimization is performed, considering the upper and lower bound for the optimization variables of Table 1. Given that Metop-A is on a SSO, the following constraints were considered:

- Local solar time of the ascending node must be maintained within 15 minutes from the reference value;
- The error on the angular separation of tracks at the equator shall be less than $\Delta l = 360/R$ deg, where R is the number of revolutions per cycle.

The results of the simulation are represented in Figure 2, where each cross corresponds to a point on the Pareto front. The top left graph represents how the mean and minimum distance increases (i.e. $f_2(\boldsymbol{x})$ decreases) as a function of the maneuver Δv. The top right plot instead represents the Pareto front on the plane $(\Delta v, P_c)$. The graph on the left bottom is obtained from the last combination of objective functions not associated with constraints. To lower collision probability below 10^{-4} a burn of at least 0.03 m/s is required. It can be observed that the two graphs on the top conveys similar results: the reason is that only one conjunction is found below the threshold R in this case for any CAM maneuver on the Pareto front. The last graph in Figure 2, on the bottom right, shows the error on the longitude after 412 revolution, i.e. after one cycle. The error is within the bounds $\pm\Delta l$, here represented by the dashed lines. For all Pareto optimal solutions no violations of the constraints are found for the 29 days following the CAM.

The solutions $\boldsymbol{x}$ on the Pareto front are represented in Figure 3. On the left the maneuver Δv is plotted against the maneuver execution time t_m. It can be observed that all maneuver capable of lowering the most collision probability have to be performed between 0.6 and 0.3 revolutions prior to the close conjunction†. In Figure 3(b) the direction and module of the associated $\Delta \boldsymbol{v}$ are plotted.

*available from `http://www.space-track.org/`

†Note that $t_m = 0$ means executing the maneuver exactly at the TCA and $t_m = 1$ one revolution before

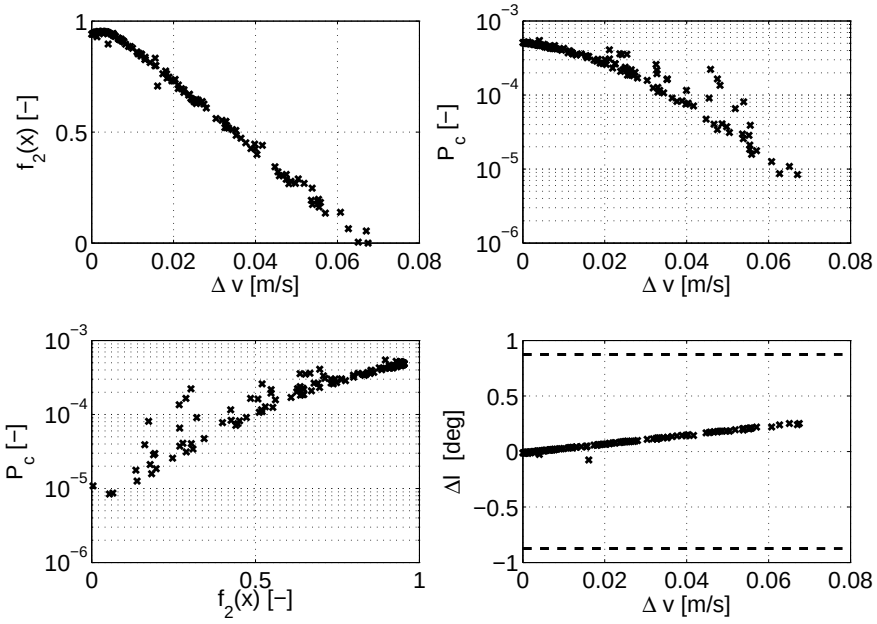

Figure 2. Pareto front for LEO collision avoidance maneuver optimization with MOPSO

The darkest vectors, which correspond to lower probabilities, are mainly aligned on the along-track direction. According to the results, if a collision probability around 10^{-5} is acceptable, then a CAM with $\Delta \boldsymbol{v} = [-2; -64; 8]$ mm/s can be performed 0.458 revolutions before the TCA (the collision probability becomes $P_c = 1.083 \times 10^{-5}$).

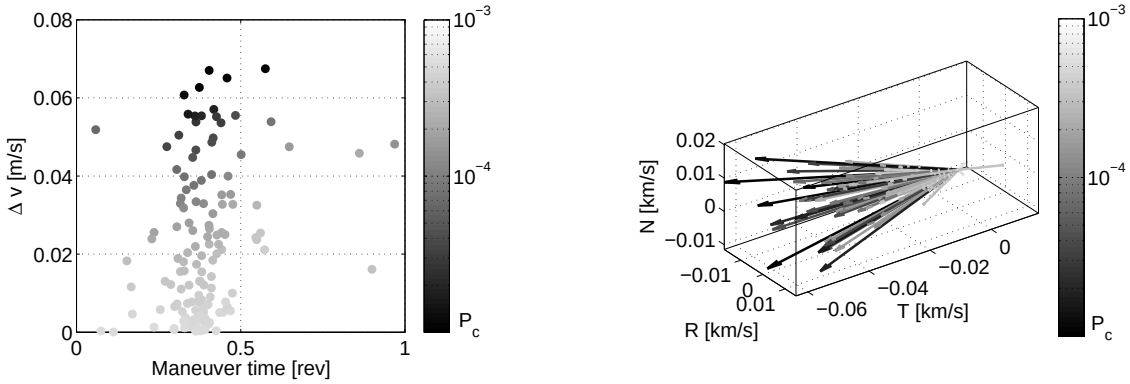

(a) Maneuver time and Δv

(b) Maneuver $\Delta \boldsymbol{v}$ in Metop-A RTN frame

Figure 3. LEO Collision avoidance maneuver on the Pareto front. Color of dots and vectors are associated with the corresponding collision probability

GEO case

A conjunction between the GEO Korean satellite COMS and Russian GSO satellite Raduga 1-7 is analyzed. COMS occupies the 128.2 ± 0.05 deg E slot, whereas the second is found inside the

128.0 ± 0.5 deg E region. Close conjunctions between the satellites can thus occur twice a day for a few days when, due to orbit evolution, the two are both around 128.2 deg E longitude. The close conjunction here analyzed occurred on 2011/07/02 at 23:14:17 UTC, one day after TLE epoch.[28] Using TLE available from Space-Track the DCA is equal to 1.676 km, with a radial, along-track, and out-of-plane separation of 1.006, 1.339, and 0.062 km respectively. The relative velocity at the TCA is 282 m/s, in the out-of-plane direction with respect to COMS. The nominal collision probability for the close conjunction is $P_c = 4.274 \times 10^{-4}$.

The following constraints are considered for the CAM optimization

- Longitude of COMS should must within ± 0.5 deg
- Latitude of COMS should must within ± 0.5 deg

The Pareto front obtained considering the objective function vector $\boldsymbol{f}(\boldsymbol{x})$ is represented in Figure 4. Due to the presence of multiple conjunctions the points are more spread: without the CAM there is indeed another close encounter occurring 12h after, on 2011/08/02 at 11:12:13 with a relative distance of 1.358 km and $P_c = 1.394 \times 10^{-4}$. Since P_c is computed for the global minimum only, the value of $f_3(\boldsymbol{x})$ changes according to the global minimum, which can be either close to the first or second one based on the maneuver.

The graph on the bottom right is the Pareto front projection on the plane (Δv,t_{in}). It is interesting to notice how the maneuver can be truly effective not only in increasing miss-distance but also as a station keeping maneuver. Without any CAM or station keeping maneuver the satellite is estimated to remain into the GEO slot for 21.5 days only, whereas the maneuver can increase this time up to 55 days.

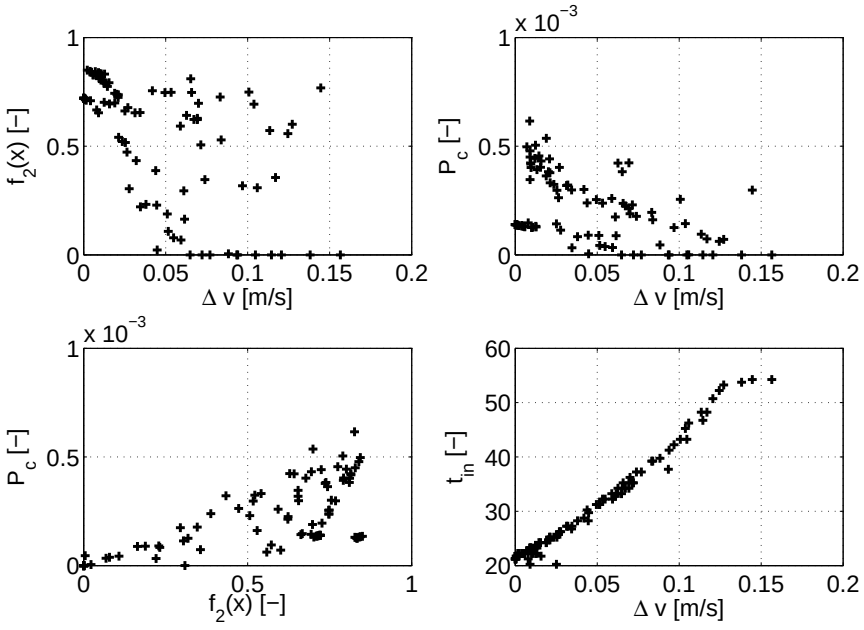

Figure 4. Pareto front for GEO collision avoidance maneuver optimization with MOPSO

The Pareto efficient CAMs are plotted in Figure 5. It can be observed in Figure 5(a) that the Δv required to lower probability down to 10^{-5} increases as t_m gets closer to the close conjunction. Figure 5(b) shows that a burn in the $-\hat{\boldsymbol{t}}$ direction is more efficient, even if the other components are not negligible. In this case two CAMs strategies can be selected from the optimization results: the first would be to perform a maneuver with the minimum consumption of fuel that guarantees a collision probability around 10^{-5} as for the LEO case. The CAM performed 0.806 revs. before the TCA with $\Delta \boldsymbol{v} = [11; -43; -8]$ mm/s meets this requirements since the collision probability becomes $P_c = 4.940 \times 10^{-6}$. Another possibility would be to perform a maneuver with a slightly larger Δv that guarantees a larger stay in the GEO slot. For example with a $\Delta \boldsymbol{v} = [-17; -118; -16]$ mm/s executed 0.486 orbits before the close conjunction allows the spacecraft to remain into the latitude/longitude slot for 50.7 days instead of the 29.7 day of the previous CAM.

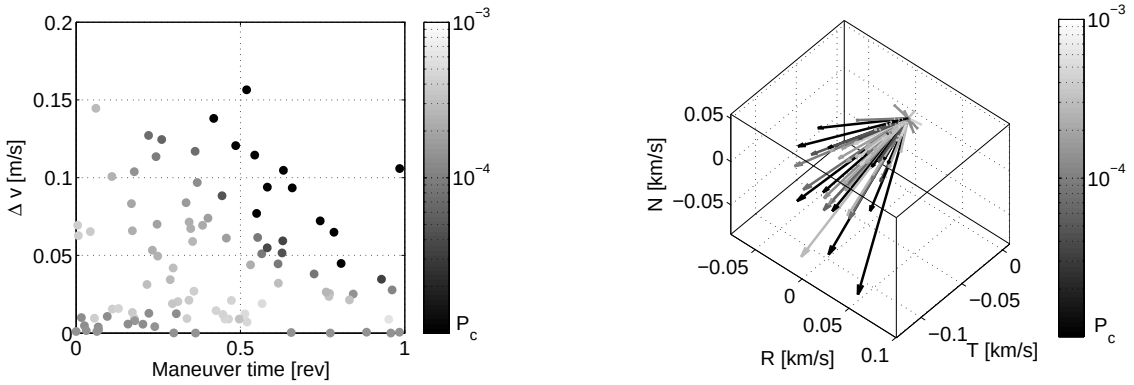

(a) Maneuver time and Δv

(b) Maneuver $\Delta \boldsymbol{v}$ in Metop-A RTN frame

Figure 5. Collision avoidance maneuver on the Pareto front. Color of dots and vectors are associated with the corresponding collision probability

An additional test is performed to understand whether another set of objective functions can give better results when dealing with more than one close conjunction with the same object. In this case the objective function $f_2(\boldsymbol{x})$ was not considered and $f_3(\boldsymbol{x})$ is modified to take into account the cumulative collision probability of all conjunctions below threshold R. The resulting Pareto front is represented in Figure 6. As before it can be observed that the CAM are able to act as station keeping maneuvers and the graph relating collision probability and Δv does not show two different probability levels as in Figure 4.

The obtained solution $\boldsymbol{x}_i$ are plotted in Figure 7. In this case all CAM that are more effective in reducing collision probability must be executed at least 0.5 orbits before the close approach and all vectors have a prevalent along-track component. As before, two possible CAM can be identified. The one lowering to zero collision probability with the lowest fuel consumption consists in a maneuver with direction $\Delta \boldsymbol{v} = [18; -44; -15]$ mm/s to be executed 0.862 revolutions before the close conjunction. The second one, that requires more fuel but allows a longer stay in the GEO box (49.5 days instead of the 30 days achievable with the previous maneuver), has to be performed 0.557 orbits before the TCA with $\Delta \boldsymbol{v} = [-35; -116; -19]$ mm/s. It is worth noting that the two CAM are really close to the one obtained with the previous strategy with four objective functions. The two approaches seems equivalent, anyway it has to be taken into account that often collision probability estimates are not reliable, since no accurate estimation of debris uncertainties

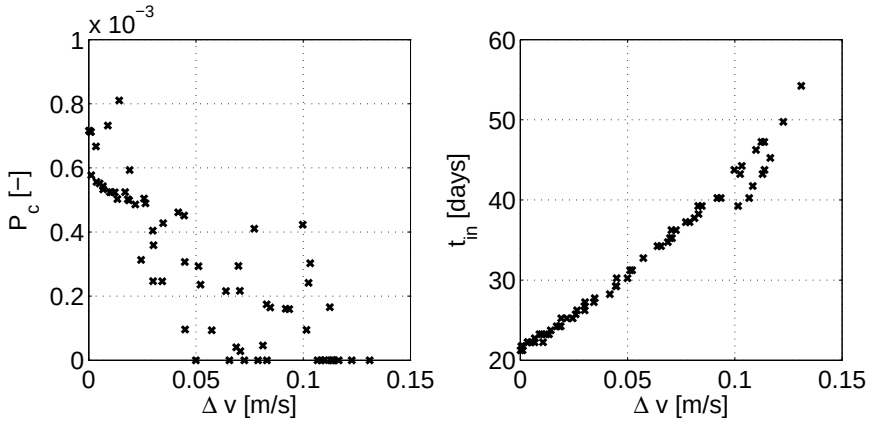

Figure 6. Pareto front for GEO collision avoidance maneuver optimization with MOPSO

are available for TLE. For real satellite operations more accurate propagators and data coming from optical or radar tracking should be used for these estimations.

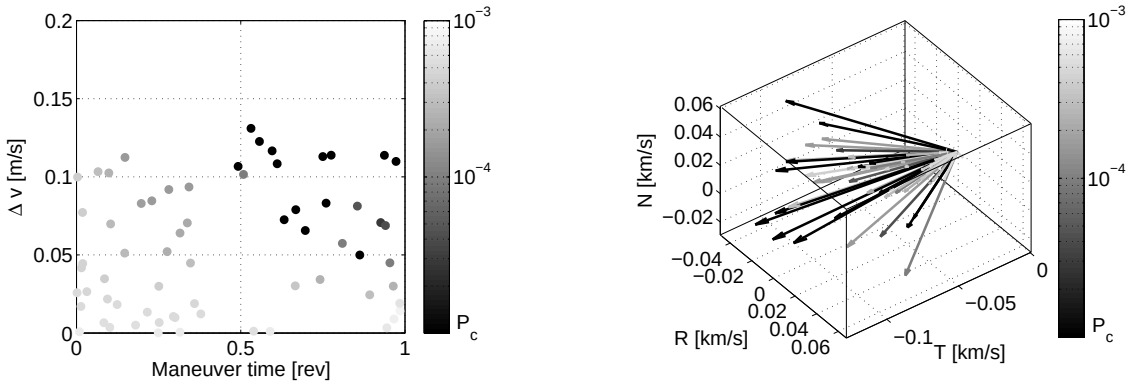

(a) Maneuver time and Δv

(b) Maneuver $\Delta \boldsymbol{v}$ in Metop-A RTN frame

Figure 7. Collision avoidance maneuver on the Pareto front for GEO. Color of dots and vectors are associated with the corresponding collision probability

The evolution of the latitude and longitude after the two CAM are plotted in Figure 8. It can be observed how the first CAM acts only marginally to the longitude shift behavior, whereas the second one has a larger impact, inverting the drift of the satellite from East to West after the maneuver, thus increasing the time inside the GEO slot.

CONCLUSIONS

A method for CAM design using a Multi-Objective Particle Swarm Optimizer was developed. The method relies on a conjunction identification algorithm, based on rigorous global optimizer COSY-GO and SGP4/SDP4 that computes all stationary points of the relative distance within a time window, and Alfano's method for collision probability computation. Three objective functions were defined to achieve the goal of increasing miss-distance between the objects involved in the close conjunction, reducing the collision risk, and minimizing fuel consumption at the same time.

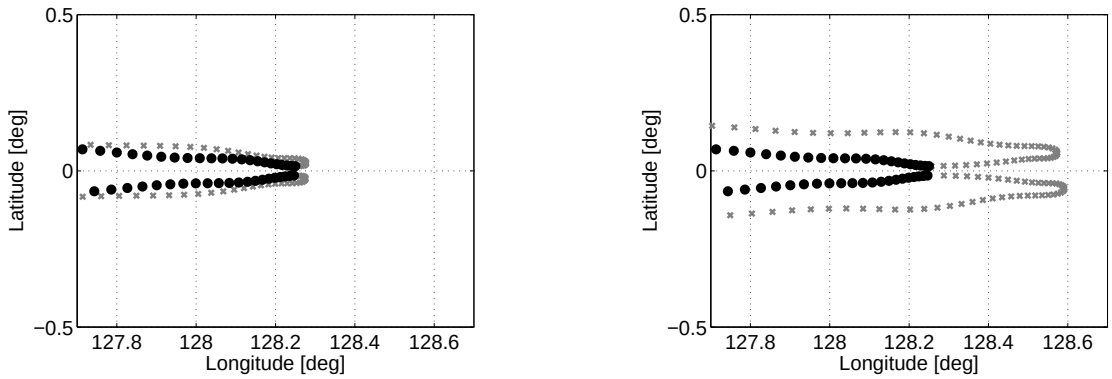

(a) CAM A

(b) CAM B

Figure 8. Evolution of latitude and longitude of COMS inside ± 0.5 deg GEO slot. Time step is 0.5 revolutions, black dots are computed from the nominal trajectory, the grey cross after CAM execution.

Another objective function was defined to take into account the mission constraint, checking that they are not violated for a given time. The method allows for the computation of optimal maneuver time and $\Delta \boldsymbol{v}$, which is not limited to the along-track direction and has a maximum magnitude of 1 m/s.

Two close conjunctions, one in LEO and one in GEO, for which a collision avoidance maneuver was performed were tested. In both cases, it was possible to identify a CAM capable of reducing collision risk below a given threshold and maintaining the satellite inside the station keeping area. For the GEO case, in particular, it was possible not only to increase the miss-distance but also to select a maneuver capable of performing some station keeping, increasing from 20 days to 50 days the time within the latitude-longitude box.

Further efforts will be devoted to the use of a numerical propagator, since SGP4/SDP4 error on position can become really large after a few days of propagations. More simulations should be performed, considering different mission constraints and taking into account limitations on direction of maneuver. Another interesting scenario, which could be studied with multi-objective optimization, is the analysis of conjunctions with more than one debris in order to design a maneuver that can reduce the cumulative collision risk with those objects.

REFERENCES

[1] F. La Porte and E. Sasot, "Operational management of collision risks for LEO satellites at CNES," *Space-Ops 2008 Conference*, 2008. , Paper AIAA-2008-3409.

[2] T. Flohrer, H. Krag, and H. Klinkrad, "ESA's process for the identification and assessment of high-risk conjunction events," *Advances in Space Research*, Vol. 44, No. 3, 2009, pp. 355–363.

[3] H. Klinkrad, J. R. Alarcon, and N. Sanchez, "Collision avoidance for Operational ESA satellites," *4th European Conference on Space Debris* (D. Danesy, ed.), Vol. 587 of *ESA Special Publication*, August 2005.

[4] R. P. Patera and G. E. Peterson, "Space vehicle maneuver method to lower collision risk to an acceptable level," *Journal of guidance, control, and dynamics*, Vol. 26, No. 2, 2003, pp. 233–237.

[5] C. Bombardelli, "Analytical formulation of impulsive collision avoidance dynamics," *Celestial Mechanics and Dynamical Astronomy*, 2013, pp. 1–16.

[6] S.-C. Lee, H.-D. Kim, and J. Suk, "Collision avoidance maneuver planning using GA for LEO and GEO satellite mainteined in keeping area," *International Journal of Aeronautical and Space Sciences*, Vol. 13, No. 4, 2012, pp. 474–483.

[7] E.-H. Kim, H.-D. Kim, and H.-J. Kim, "Optimal Solution of Collision Avoidance Maneuver with Multiple Space Debris," *Journal of Space Operations*, Vol. 9, No. 3, 2012, pp. 20–31.

[8] J. Kennedy and R. C. Eberhart, *Swarm Intelligence*. San Francisco, CA, USA: Morgan Kaufmann Publishers Inc., 2001.

[9] R. Armellin, A. Morselli, P. Di Lizia, and M. Lavagna, "Rigorous computation of orbital conjunctions," *Advances in Space Research*, Vol. 50, No. 5, 2012, pp. 527 – 538, 10.1016/j.asr.2012.05.011.

[10] R. B. Kearfott, *Rigorous Global Search: Continuous Problems*. Dordrecht: Kluwer Academic Publishers, 1996.

[11] K. Makino and M. Berz, "Efficient Control of the Dependency Problem Based on Taylor Model Methods," *Reliable Computing*, Vol. 5, No. 1, 1999, pp. 3–12.

[12] K. Makino, *Rigorous Analysis of Nonlinear Motion in Particle Accelerators*. PhD thesis, Michigan State University, East Lansing, 1998.

[13] M. Berz, C. Bischof, G. Corliss, and A. Griewank, *Computational Differentiation: Techniques, Applications, and Tools*. Philadelphia: SIAM, 1996.

[14] A. Griewank and G. Corliss, *Automatic Differentiation of Algorithms*. Philadelphia: SIAM, 1991.

[15] M. Berz and K. Makino, *COSY INFINITY Version 9 Reference Manual*. Michigan State University, East Lansing, MI 48824, 2006. MSU Report MSUHEP-060803.

[16] M. Berz, *Modern Map Methods in Particle Beam Physics*, Vol. 108. New York: Academic Press, 1999.

[17] K. Makino and M. Berz, "Taylor models and other validated functional inclusion methods," *International Journal of Pure and Applied Mathematics*, Vol. 4, No. 4, 2003, pp. 379–456.

[18] M. Berz, K. Makino, and Y. Kim, "Long-term Stability of the Tevatron by Verified Global Optimization," *Nuclear Instruments and Methods*, Vol. A558, No. 1, 2006, pp. 1–10.

[19] K. Makino and M. Berz, "Verified Global Optimization with Taylor Model-based Range Bounders," *Transactions on Computers*, Vol. 4, No. 11, 2005, pp. 1611–1618.

[20] M. R. Akella and K. T. Alfriend, "Probability of collision between space objects," *Journal of Guidance, Control, and Dynamics*, Vol. 23, No. 5, 2000, pp. 769–772.

[21] N. Bèrend, "Estimation of the probability of collision between two catalogued orbiting objects," *Advances in Space Research*, Vol. 23, No. 1, 1999, pp. 243–247.

[22] R. P. Patera, "General method for calculating satellite collision probability," *Journal of Guidance, Control, and Dynamics*, Vol. 24, No. 4, 2001, pp. 716–722.

[23] T. Flohrer, H. Krag, H. Klinkrad, B. Bastida Virgili, and C. Früh, "Improving ESA's Collision Risk Estimates by an Assessment of the TLE Orbit Errors of the US SSN Catalogue," *Proceedings of the 5th European Conference on Space Debris, Darmstadt, Germany*, Vol. ESA SP-672, 2009.

[24] S. Alfano, "A numerical implementation of spherical object collision probability," *Journal of the Astronautical Sciences*, Vol. 53, No. 1, 2005, pp. 103–109.

[25] K. Deb, "Evolutionary algorithms for multi-criterion optimization in engineering design," *Evolutionary Algorithms in Engineering and Computer Science*, Vol. 2, 1999, pp. 135–161.

[26] G. Coath and S. Halgamuge, "A comparison of constraint-handling methods for the application of particle swarm optimization to constrained nonlinear optimization problems," *Congress on Evolutionary Computation CEC '03*, Vol. 4, 2003, pp. 2419–2425.

[27] D. Làzaro and P. L. Righetti, "Evolution of EUMETSAT LEO conjunction events in handling operations," *Proceedings of SpaceOps 2012 Conference*, 2012.

[28] B. Lee, Y. Hwang, H. Kim, and B. Kim, "GEO Satellite Collision Avoidance Maneuver Due to the Close Approach of an Inclined GSO Satellite," *European Space Surveillance Conference*, Madrid, Spain, 7–9 June 2011.